

Electronic Supplementary Information (ESI)

Mixed Lead–Tin Perovskite Films with $>7 \mu\text{s}$ Charge Carrier Lifetimes Realized by Maltol Post-Treatment

Shuaifeng Hu, Minh Anh Truong, Kento Otsuka, Taketo Handa, Takumi Yamada, Ryosuke Nishikubo, Yasuko Iwasaki, Akinori Saeki, Richard Murdey, Yoshihiko Kanemitsu, and Atsushi Wakamiya*

E-mail: wakamiya@scl.kyoto-u.ac.jp

Table of Contents

Experimental procedures	S3–5
Synthesis of Sn(II)-halide complexes	S6
X-ray single crystal structural analysis	S7–12
Pictures of the single crystals	S13
Top-view of perovskite films used for composition screening	S14
PL spectra and TRPL decay curves of perovskite films used for composition screening	S15
Photoluminescence and band energy levels of the perovskite films used for screening	S16
Top-view and cross-sectional SEM images of the perovskite films	S17
XRD peak intensity and FWHM of (100) peak of the perovskite films	S18
Excitation intensity dependence of PL spectra and TRPL decay curves	S19
TRPL decay of the perovskite film treated with TM-DHP and maltol	S20
TRMC transients of perovskite films with TM-DHP and maltol treatment	S21
Distributions of solar cell device performance parameters	S22
Data used to calculate the spectral mismatch	S23
Variations of parallel resistance as a function of applied voltage	S24
The hole and electron trap densities estimated from the SCLC measurements	S25
TRPL decay curves of the perovskite films	S26
Kojic acid treated perovskite	S27
Dark J – V curves of the PSCs	S28
MPPT of the representative device prepared with TM-DHP and maltol treatment	S29
Photoelectron yield spectroscopy (PYS) results	S30
NMR data of SnI(maltol) and maltol	S31–32
References	S33

Experimental section

Materials

Unless otherwise stated, all materials were used as received without further purification. Methylammonium iodide (MAI, 99.99%), formamidinium iodide (FAI, 99.99%), bathocuproine (BCP), lead(II) iodide (PbI₂, 99.99%, trace metals basis), cesium iodide (CsI), and 3-hydroxy-2-methyl-4-pyrone (maltol) were purchased from Tokyo Chemical Industry Co., Ltd. (TCI). Lead(II) thiocyanate (Pb(SCN)₂, 99.5% trace metals), tin(II) fluoride (SnF₂, 99%), and tin(II) iodide (SnI₂, beads, 99.99%, trace metals basis) were purchased from Sigma-Aldrich Co., Ltd. (Sigma-Aldrich). Poly(3,4-ethylenedioxythiophene):polystyrene sulfonate (PEDOT:PSS) aqueous solution (Clevious PVP AI 4083) was purchased from Heraeus Co., Ltd. C₆₀ (sublimed, 99.99%) was purchased from ATR Company. Dehydrated dimethylsulfoxide (DMSO, super dehydrated) was purchased from FUJIFILM Wako Pure Chemical Co., Ltd. Dimethylformamide (DMF) chlorobenzene, and toluene were purchased from Kanto Chemical. Co., Inc. All of these solvents were degassed by Ar gas bubbling for 1 h and further dried over molecular sieves in an Ar-filled glove box (O₂, H₂O < 0.1 ppm) before use. Glass-FTO substrates (10 Ω sq⁻¹) and quartz glass substrates were purchased from Asahi Glass Co., Ltd. Glass-ITO substrate (10 Ω sq⁻¹) were purchased from Geomatec Co., Ltd. 1,4-bis(trimethylsilyl)-2,3,5,6-tetramethyl-1,4-dihydropyrazine (TM-DHP) was synthesized according to our previously reported literature.¹

Equipment and Characterization

¹H and ¹³C NMR spectra were recorded on Bruker Avance-400 spectrometer (400 MHz for ¹H NMR, 101 MHz for ¹³C NMR). The NMR chemical shifts are reported in ppm relative to the residual protons and carbons of DMSO-*d*₆ ($\delta = 2.50$ ppm in ¹H NMR, $\delta = 39.52$ ppm in ¹³C NMR).

Photoelectron yield spectroscopy (PYS) measurements were carried out using a BUNKOUKEIKI BIP-KV201 under vacuum ($\sim 10^{-3}$ Pa). Perovskite film samples for PYS measurements were prepared by deposition of the precursor solution on the surface of PEDOT:PSS with ITO as substrates in an Ar-filled glove box and transferred to the chamber for PYS measurement without exposure to air.

For the time-resolved photoluminescence (TRPL) measurements, in case of component screening, the samples were excited by a picosecond pulsed light with a wavelength of 406 nm (Advanced Laser Diode System), and beam intensity was set at 2.4×10^{13} photons cm⁻² ($12 \mu\text{J cm}^{-2}$) with the excitation frequency of 100 kHz. In case of detail study, the samples were excited by a picosecond pulsed light with a wavelength of 688 nm (Advanced Laser Diode System), and the excitation energy was set at 3.5×10^{11} photons cm⁻² (100 nJ cm^{-2}) with the excitation frequency of 10 kHz. The PL signals were recorded using an avalanche photodiode (ID Quantique) and a time-correlated single photon counting board (PicoQuant). The PL lifetimes were obtained by fitting the PL decay curve with an exponential function: $y = A\exp(-(x - x_0)/\tau)$ (τ is carrier lifetime). The PL spectra were recorded using an InGaAs array detector equipped with a monochromator (Princeton Instruments). The samples were kept in an Ar-filled metallic box for the whole process to avoid oxygen contamination and degradation.

Scanning electron microscopy (SEM) was performed with an S8010 (Hitachi High-Technologies Co.).

X-ray Single crystal structure analysis was performed on a Bruker Single Crystal CCD X-ray Diffractometer SMART APEX II with Mo K α radiation ($\lambda = 0.71073 \text{ \AA}$) and graphite monochromator (Bruker Co.). The structures were solved by direct method and were refined with *SHELXL-2018/1*.²

Thin film X-ray diffraction (XRD) measurements were performed on a Rigaku RINT 2500 (Rigaku Co.) with Cu K α radiation ($\lambda = 1.5406 \text{ \AA}$). All the samples were scanned with $2\theta = 5^\circ - 50^\circ$ with a 0.05° step and 0.2 s integration time. The power supply was operated at 300 mA and 40 kV.

X-ray photoelectron spectroscopy (XPS) was recorded with a JPS-9010 (JEOL Co., Ltd.) instrument. Perovskite film samples for XPS measurements were prepared in an Ar-filled glove box and transferred to the XPS chamber through an Ar-filled transfer vessel in order to avoid oxygen contamination.

Photocurrent–voltage (*J–V*) curves for PSCs were measured in a nitrogen-filled glove box (O₂, H₂O < 0.1 ppm) with an OTENTO-SUN-P1G solar simulator (BUNKOUKEIKI Co., Ltd.) and a Keithley 2400 source meter with an active area of 0.0985 cm². The light intensity of the illumination source was calibrated using a standard silicon photodiode. External quantum efficiency (EQE) and internal quantum efficiency (IQE) spectra were measured by a SMO-250III system equipped with an SM-250 diffuse reflection unit (BUNKOUKEIKI Co., Ltd.). The light intensity of the illumination source was calibrated with a standard SiPD S1337-1010BQ silicon photodiode.

Flash-photolysis time-resolved microwave conductivity (TRMC) was performed for the films prepared on a quartz substrate, which was loaded in a closed microwave resonant cavity in a N₂-filled glovebox to

prevent an exposure to air. The microwave frequency and its power were ~9 GHz and ~3 mW, respectively. A visible light pulse (500 nm) from an optimal parametric oscillator (OPO, Continuum Inc., Panther) seeded by third harmonic generation of a Nd:YAG laser (Continuum Inc., Surelite II, 5–8 ns pulse duration, 10 Hz) was used for the excitation (incident photon density $I_0 = 6.4 \times 10^{10}$ photons cm^{-2} pulse $^{-1}$). The photoconductivity ($\Delta\sigma = A^{-1} \Delta P_r P_r^{-1}$ where A is the sensitivity factor, P_r is the reflected microwave power, and ΔP_r is the change in P_r upon exposure to light) was converted into the product of the quantum yield (φ) and sum of the charge carrier mobilities $\Sigma\mu (= \mu_+ + \mu_-)$ using the relationship $\varphi\Sigma\mu = \Delta\sigma(eI_0F_{\text{light}})^{-1}$, where e and F_{light} are the electron charge and correction (or filling) factor, respectively. The experiments were performed at room temperature.

Impedance spectroscopy data were obtained in inert atmosphere under AM 1.5G simulated solar radiation, using an Agilent E4990A impedance analyzer. Scans were taken from 20 Hz to 20 MHz, with a 30 mV oscillator voltage, for bias voltages from 0 to 0.9 V in 0.1 V steps.

X-ray Single Crystal Structure Analysis

The crystallographic data for Sn(maltol)₂, SnBr(maltol), and SnI(maltol) have been deposited to the Cambridge Crystallographic Data Centre (CCDC) as supplementary publication number CCDC–2080061, CCDC–2080062, and CCDC–2080063, respectively. Data files can be obtained free of charge from the CCDC via www.ccdc.cam.ac.uk/data_request/cif.

Fabrication of Perovskite Films

The perovskite film preparation was conducted in an Ar-filled glove box. The Cs_{0.1}FA_{0.6}MA_{0.3}Sn_{0.5}Pb_{0.5}I₃ perovskite precursor solution was prepared by mixing CsI (93.2 mg, 0.36 mmol), FAI (371.5 mg, 2.16 mmol), MAI (171.7 mg, 1.08 mmol) SnI₂ (670.5 mg, 1.80 mmol), PbI₂ (829.8 mg, 1.80 mmol), Pb(SCN)₂ (11.6 mg, 0.04 mmol), and SnF₂ (28.2 mg, 0.18 mmol) in mixed solvents of 0.5 mL DMSO and 1.5 mL DMF to reach a concentration of 1.8 M. After stirring the solution at 45 °C for 30 min, a solution of reductant TM-DHP in DMF (1.0 M, 19 μL) was added to reach the amount of 1.0 mol% for SnI₂. The color of precursor solution changed from clear yellow to yellowish-gray, and turned back to clear yellow after stirring the solution at 45 °C for ca. 15 min. After stirring for another 15 min, the solution was filtered through a 0.20 μm PTFE filter. 200 μL of the precursor solution at room temperature were used for spin coating. The perovskite films were fabricated with a two-step spin coating procedure. The first step was 1000 rpm for 10 s with an acceleration of 200 rpm s $^{-1}$. The second step was 4000 rpm for 40 s with an acceleration of 1000 rpm s $^{-1}$. Chlorobenzene (400 μL) at room temperature was dripped on the top of spinning substrate over an interval of 1 s during the second spin coating step at 20 s before the end of the procedure. Then, the substrate was immediately annealed on a hot plate. The annealing of the films was processed at 100 °C for 10 min and 65 °C for over 10 min. Thin films of other Cs_xFA_yMA_{1-x-y}Sn_{0.5}Pb_{0.5}I₃ perovskites and different concentration were also fabricated with similar procedure by using corresponding equivalence of starting materials. 1.0 mg mL $^{-1}$ of maltol was dissolved in toluene for preparing the solution for surface treatment. 120 μL of maltol solution was spin coated on the perovskite surface at 4000 rpm for 20 s, and then annealed at 65 °C for 2 min.

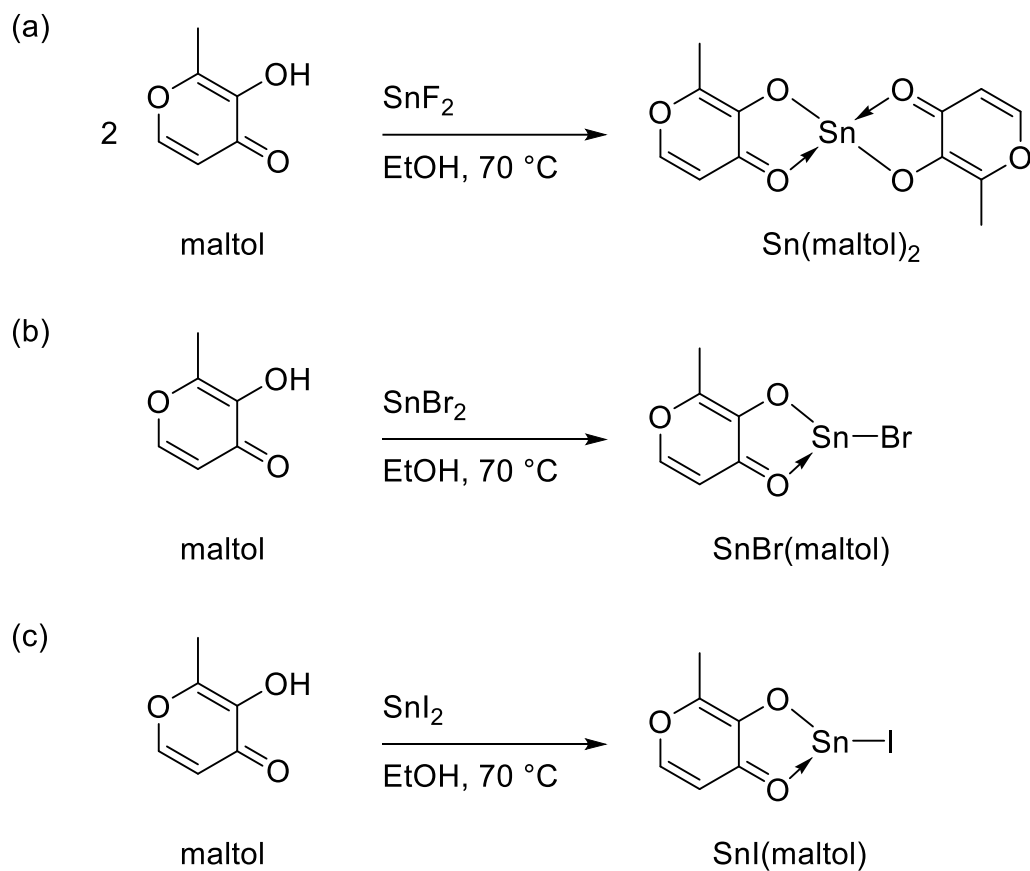
The devices for space-charge-limited current (SCLC) measurement were prepared. The perovskite layers were deposited with the same processes modified for the PSCs fabrication. PEDOT:PSS was spin coated on the FTO substrate at 500 rpm for 10 s and 3000 rpm for 30 s, and then annealed at 140 °C for 20 min. For completing the hole-only devices, 150 μL PTAA solution (20 mg/mL in chlorobenzene, doped with 1 wt% F4-TCNQ) was spin-coated onto the perovskite films fabricated on the PEDOT:PSS-coated substrates at 2000 rpm for 20 s with an acceleration of 400 rpm s $^{-1}$, and the films were immediately annealed at 70 °C for around 5 min. For the electron-only devices, double-sided C₆₀ layers (30 nm) were sequentially deposited by thermal evaporation. Finally, 100 nm of silver was deposited through a metallic aperture mask to form the metal electrode for all the samples.

Fabrication of Solar Cell Devices

Glass/FTO substrates (Asahi Glass Co., Ltd., Japan) were etched with zinc powder and HCl aq. (6 M in de-ionized water), then consecutively cleaned with water, acetone, detergent solution (Semico Clean 56, Furuuchi chemical), water, and isopropyl alcohol with 15 min ultrasonic bath, followed by drying with an air gun. Finally, the organic residues on substrates were removed by plasma treatment. PEDOT:PSS dispersion in water was filtered through a 0.45 μm PVDF filter and then spin coated on the FTO substrate at 500 rpm for 10 s and 4000 rpm for 60 s, and then annealed at 140 °C for 20 min. The substrates were transferred to an Ar-filled glove box and annealed at 140 °C for another 30 min. The perovskite layer was

fabricated on top of PEDOT:PSS following the above-mentioned procedure. Then, 20 nm of C₆₀ (0.01 nm s⁻¹) and 8 nm of BCP (0.01 nm s⁻¹) were deposited by thermal evaporation. Finally, 100 nm of silver (0.005 nm s⁻¹) was deposited through a shadow mask to form the metal electrode. The cells for the EQE measurement were encapsulated by a cover glass and sealed with AFTINNOVA-EF FD20 film (Ajinomoto Fine-Techno Co., Inc.) by heating at 70 °C for 5 min.

Results and discussion



Scheme S1. Synthetic routes for (a) Sn(maltol)₂, (b) SnBr(maltol), and (c) SnI(maltol).

Preparation of Sn(maltol)₂: SnF₂ (156.7 mg, 1.0 mmol) and maltol (252.2 mg, 2.0 mmol) were dissolved in dry ethanol (4.0 mL) at 70 °C under an inert atmosphere. The resulting solution was filtered with a membrane filter (0.45 μm, PTFE) to remove the insoluble part. The resultant solution was transferred to a vial and slowly cooled down to room temperature. After standing at room temperature for 12 h, the formed crystals were collected by filtration for single crystal characterization.

Crystal data of Sn(maltol)₂: C₁₂H₁₀O₆Sn, colorless, needle, 0.06 × 0.10 × 0.18 mm, orthorhombic, space group *Fdd2*, *a* = 18.909(2) Å, *b* = 26.360(3) Å, *c* = 4.9742(5) Å, *V* = 2479.4(4) Å³, *F*_w = 368.89, λ = 0.71073 Å, *Z* = 8, *D*_{calc} = 1.976 g/cm³, μ = 2.081 mm⁻¹, *T* = 100 K, *R*₁[*I* > 2σ(*I*)] = 0.0146, *wR*₂ (all data) = 0.0333, GOF (on *F*²) = 1.045. (CCDC: 2080061)

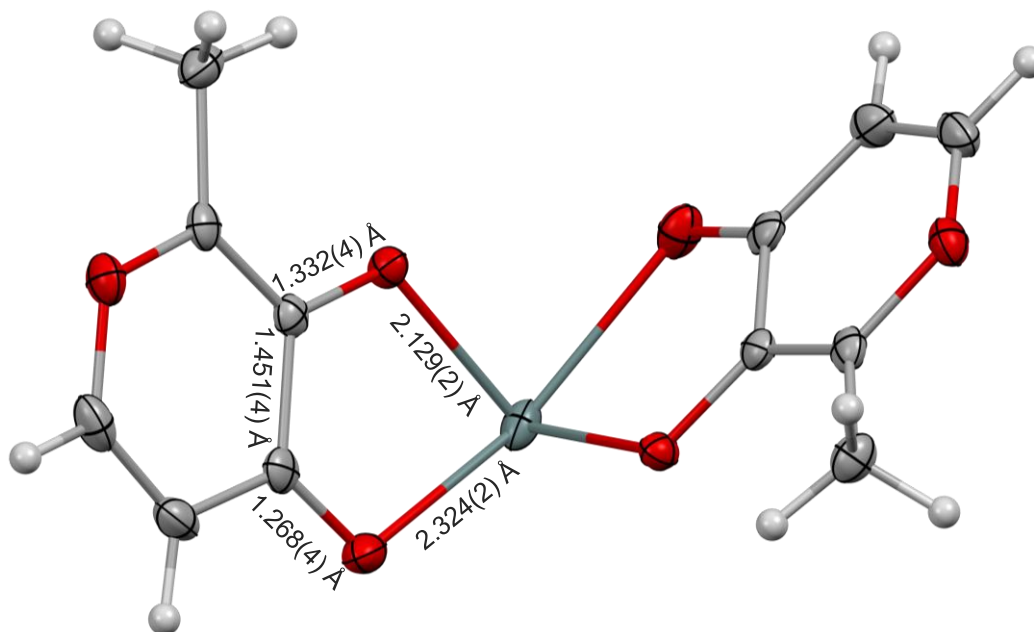


Figure S1. ORTEP drawing of Sn(maltol)₂ crystal structure with 50% thermal ellipsoids. Selected bond lengths are shown.

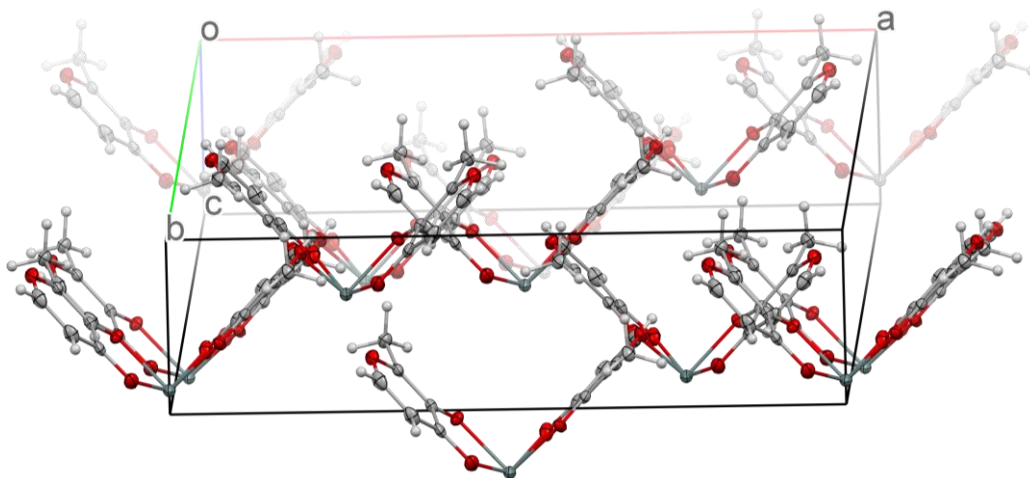


Figure S2. Crystal packing structure of $\text{Sn}(\text{malto})_2$.

Preparation of SnBr(maltol): SnBr₂ (278.5 mg, 1.0 mmol) and maltol (252.2 mg, 2.0 mmol) were dissolved in dry ethanol (13 mL) at 70 °C under an inert atmosphere. The resulting solution was filtered with a membrane filter (0.45 μm, PTFE) to remove the insoluble part. The resultant solution was transferred to a vial and slowly cooled down to room temperature. After standing at room temperature for 12 h, the formed crystals were collected by filtration for single crystal characterization.

Crystal data of SnBr(maltol): C₆H₅O₃SnBr, colorless, needle, 0.10 × 0.10 × 0.37 mm, monoclinic, space group *P*2₁/*c*, *a* = 9.4048(12) Å, *b* = 7.3958(9) Å, *c* = 11.7318(14) Å, *β* = 98.096(2)°, *V* = 807.73(17) Å³, *F*_w = 323.70, *λ* = 0.71073 Å, *Z* = 4, *D*_{calc} = 2.662 g/cm³, *μ* = 8.060 mm⁻¹, *T* = 100 K, *R*₁[*I* > 2σ(*I*)] = 0.0164, *wR*₂ (all data) = 0.0371, GOF (on *F*²) = 1.039. (CCDC: 2080062)

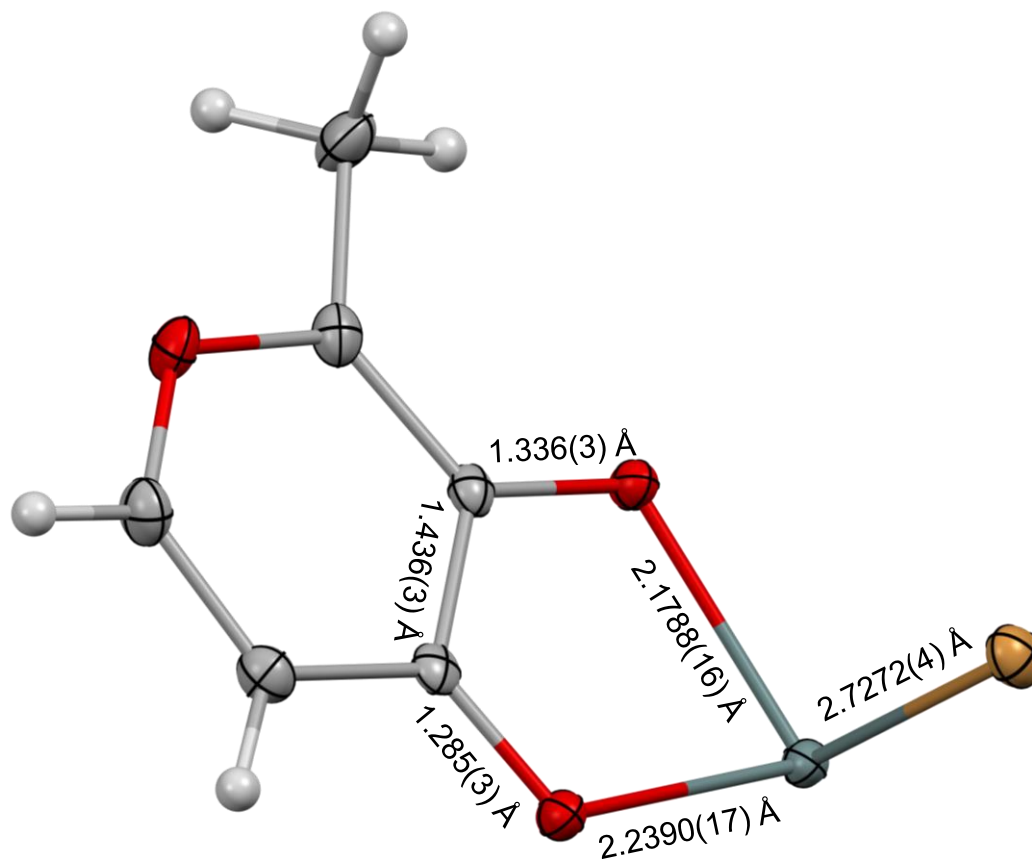


Figure S3. ORTEP drawing of SnBr(maltol) crystal structure with 50% thermal ellipsoids. Selected bond lengths are shown.

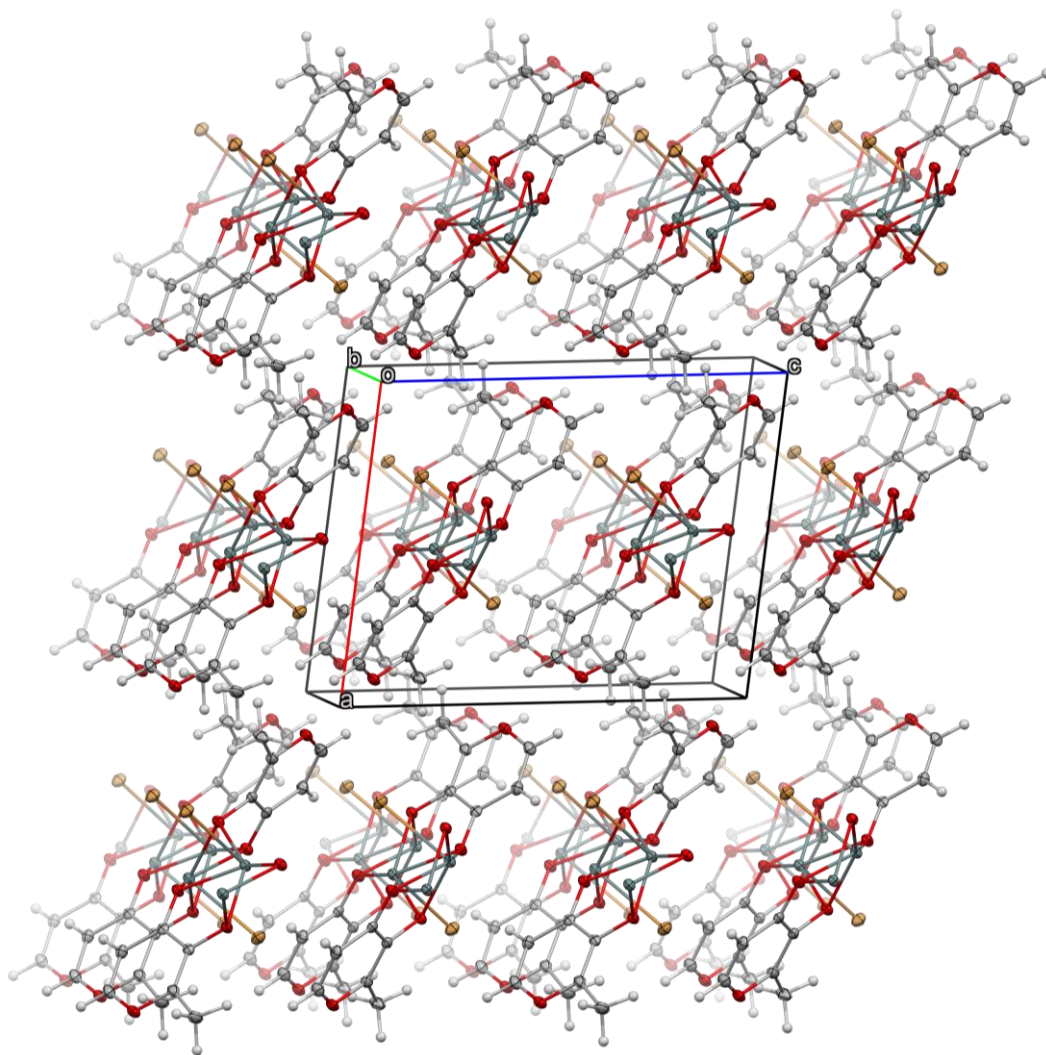


Figure S4. Crystal packing structure of SnBr(maltol).

Preparation of SnI(maltol):

SnI₂ (186.3 mg, 0.50 mmol) and maltol (63.1 mg, 0.50 mmol) were dissolved in dry ethanol (22 mL) at 70 °C under an inert atmosphere. The resulting solution was filtered with a membrane filter (0.45 μm, PTFE) to remove the insoluble part. The resultant solution was transferred to a vial and slowly cooled down to room temperature. After standing at room temperature for 12 h, the formed crystals were collected by filtration to give SnI(maltol) as pale-yellow crystals (85.6 mg, 0.23 mmol, 46% yield).

¹H NMR (400 MHz, DMSO-*d*₆): δ 8.38–8.37 (d, *J* = 5.2 Hz, 1H), 6.80–6.79 (d, *J* = 5.2 Hz, 1H), 2.46 (s, 3H).

¹³C NMR (101 MHz, DMSO-*d*₆): δ 177.47, 155.74, 153.67, 150.53, 111.22, 14.78.

SnI(maltol) was also synthesized as a major product by mixing SnI₂ and maltol in 1:2 ratio: SnI₂ (186.3 mg, 0.50 mmol) and maltol (126.1 mg, 1.0 mmol) were dissolved in dry ethanol (27 mL) at 70 °C under an inert atmosphere. The resulting solution was filtered with a membrane filter to remove the insoluble part. The resultant solution was transferred to a vial and slowly cooled down to room temperature. After standing at room temperature for 12 h, the formed crystals were collected by filtration to give SnI(maltol) as pale-yellow crystals (88.6 mg, 0.24 mmol, 48% yield).

Crystal data of SnI(maltol): C₆H₅O₃SnI, pale-yellow, needle, 0.08 × 0.10 × 0.28 mm, orthorhombic, space group *Pbca*, *a* = 7.575(1) Å, *b* = 12.2799(16) Å, *c* = 18.784(3) Å, *V* = 1747.3(4) Å³, *F*_w = 370.69, λ = 0.71073 Å, *Z* = 8, *D*_{calc} = 2.818 g/cm³, μ = 6.414 mm⁻¹, *T* = 100 K, *R*₁[*I* > 2σ(*I*)] = 0.0170, *wR*₂ (all data) = 0.0348, GOF (on *F*²) = 1.351. (CCDC: 2080063)

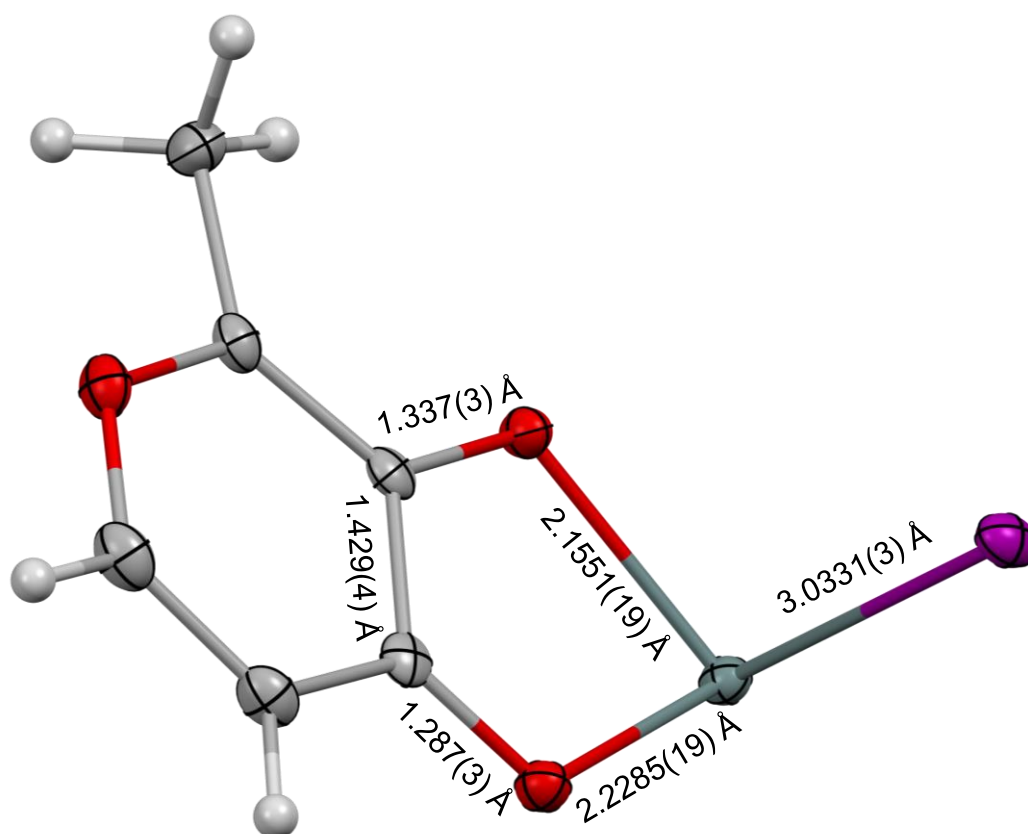


Figure S5. ORTEP drawing of SnI(maltol) crystal structure with 50% thermal ellipsoids. Selected bond lengths are shown.

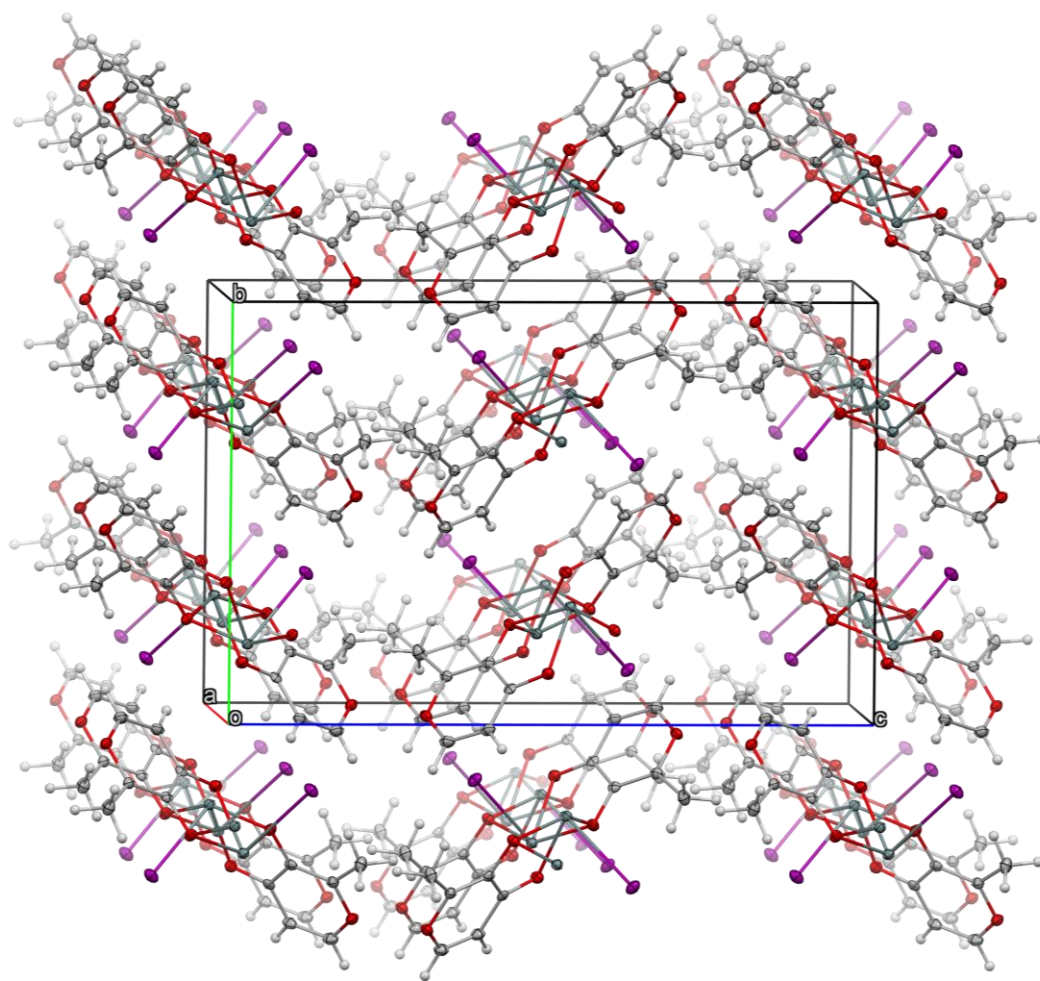


Figure S6. Crystal packing structure of SnI(maltol).

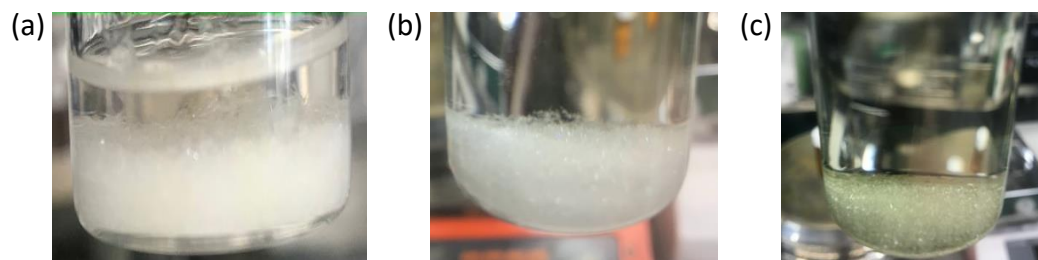


Figure S7. Pictures for the single crystals of (a) $\text{Sn}(\text{maltol})_2$, (b) $\text{SnBr}(\text{maltol})$, and (c) $\text{SnI}(\text{maltol})$.

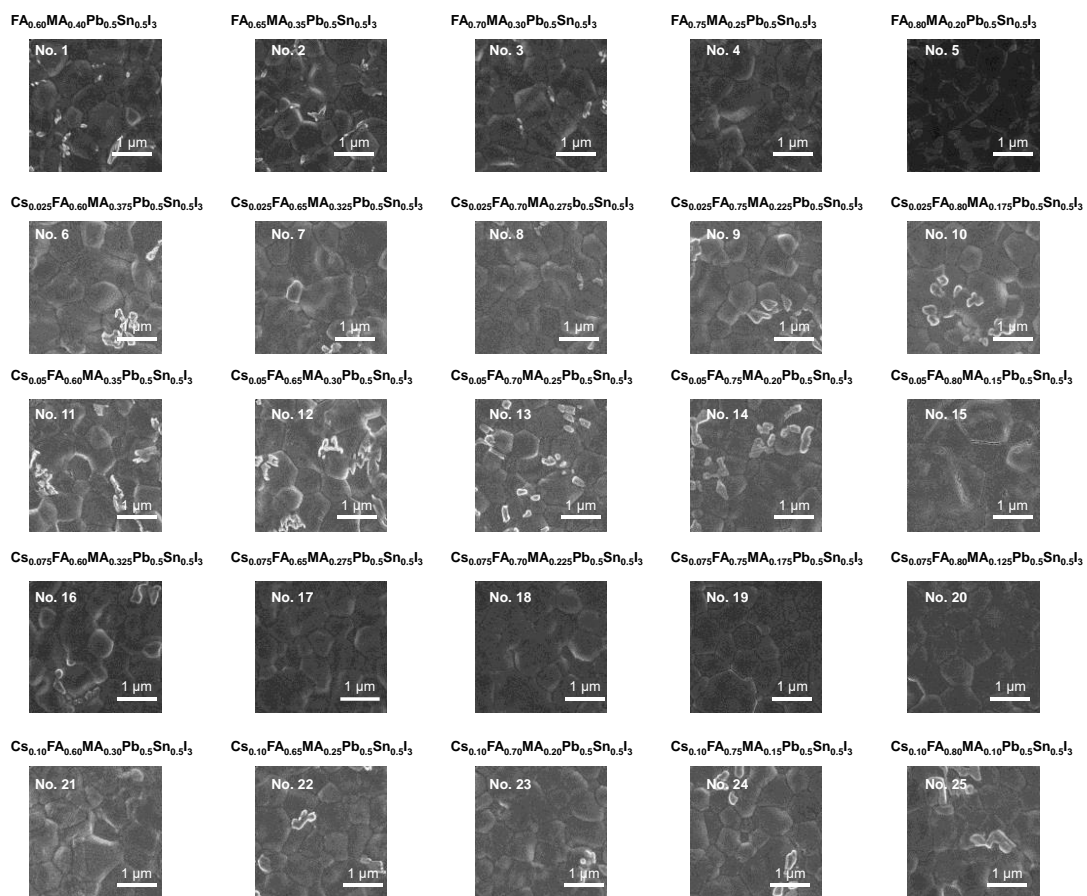


Figure S8. Top-view SEM images of perovskite films fabricated on quartz substrates. Same sample numbers were used in Figure S9 and Table S1.

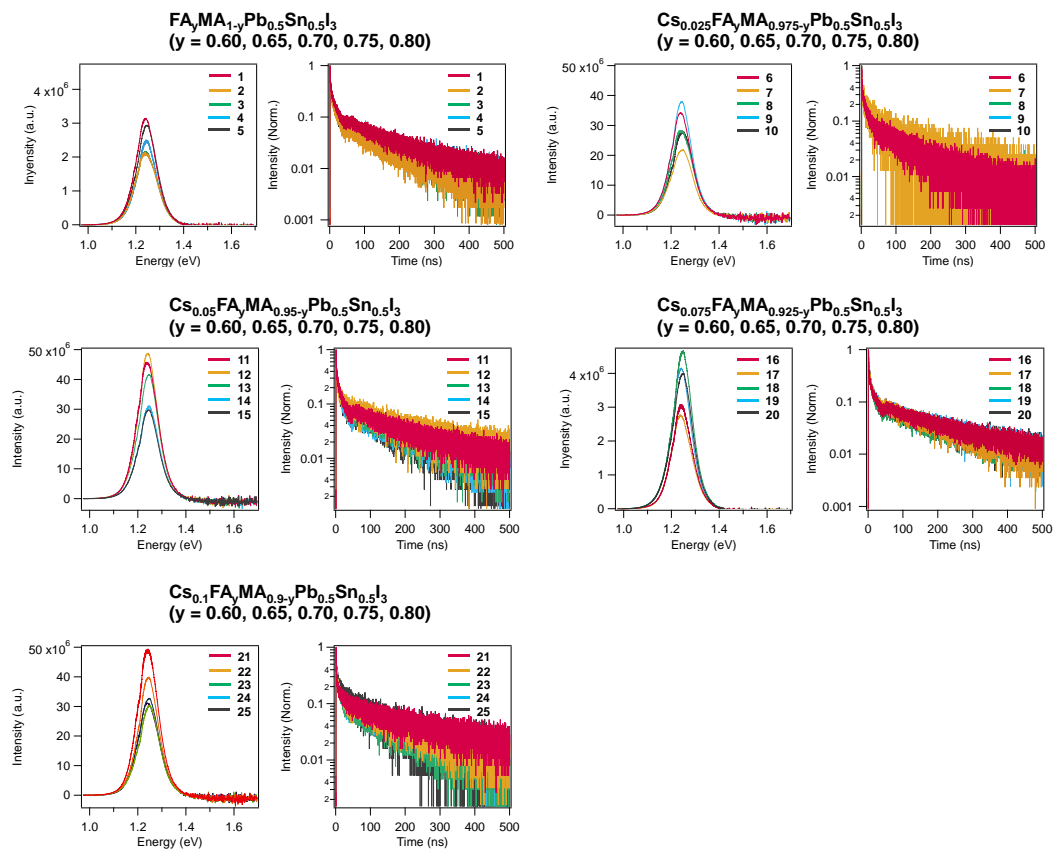


Figure S9. PL spectra and TRPL decay curves of perovskite films fabricated on quartz substrates. Detailed parameters are listed in Table S1.

Table S1. List of $\text{Cs}_x\text{FA}_y\text{MA}_{1-x-y}\text{Sn}_{0.5}\text{Pb}_{0.5}\text{I}_3$ components used for screening.

No.	Cs (x)	FA (y)	MA (1-x-y)	Bandgap (eV)	VBM (eV)	CBM (eV)	PL lifetime (ns)
1	0	0.60	0.40	1.24	-5.26	-4.02	154
2	0	0.65	0.35	1.24	-5.28	-4.04	116
3	0	0.70	0.30	1.24	-5.30	-4.06	120
4	0	0.75	0.25	1.25	-5.27	-4.03	142
5	0	0.80	0.20	1.25	-5.30	-4.06	171
6	0.025	0.60	0.375	1.24	-5.28	-4.04	112
7	0.025	0.65	0.325	1.25	-5.25	-4.01	96
8	0.025	0.70	0.275	1.24	-5.29	-4.05	129
9	0.025	0.75	0.225	1.24	-5.28	-4.04	137
10	0.025	0.80	0.175	1.24	-5.28	-4.04	146
11	0.05	0.60	0.35	1.24	-5.38	-4.14	191
12	0.05	0.65	0.30	1.24	-5.30	-4.06	179
13	0.05	0.70	0.25	1.25	-5.27	-4.03	164
14	0.05	0.75	0.20	1.25	-5.24	-3.99	157
15	0.05	0.80	0.15	1.25	-5.24	-4.00	133
16	0.075	0.60	0.325	1.24	-5.29	-4.05	196
17	0.075	0.65	0.275	1.24	-5.30	-4.06	165
18	0.075	0.70	0.225	1.26	-5.18	-3.94	183
19	0.075	0.75	0.175	1.24	-5.19	-3.95	180
20	0.075	0.80	0.125	1.25	-5.20	-3.96	207
21	0.10	0.60	0.30	1.24	-5.37	-4.13	216
22	0.10	0.65	0.25	1.25	-5.33	-4.09	171
23	0.10	0.70	0.20	1.25	-5.25	-4.00	140
24	0.10	0.75	0.15	1.25	-5.20	-3.96	175
25	0.10	0.80	0.10	1.24	-5.14	-3.90	147

Component No. 21 ($\text{Cs}_{0.10}\text{FA}_{0.60}\text{MA}_{0.30}\text{Sn}_{0.5}\text{Pb}_{0.5}\text{I}_3$) was chosen as optimal composition for this study.

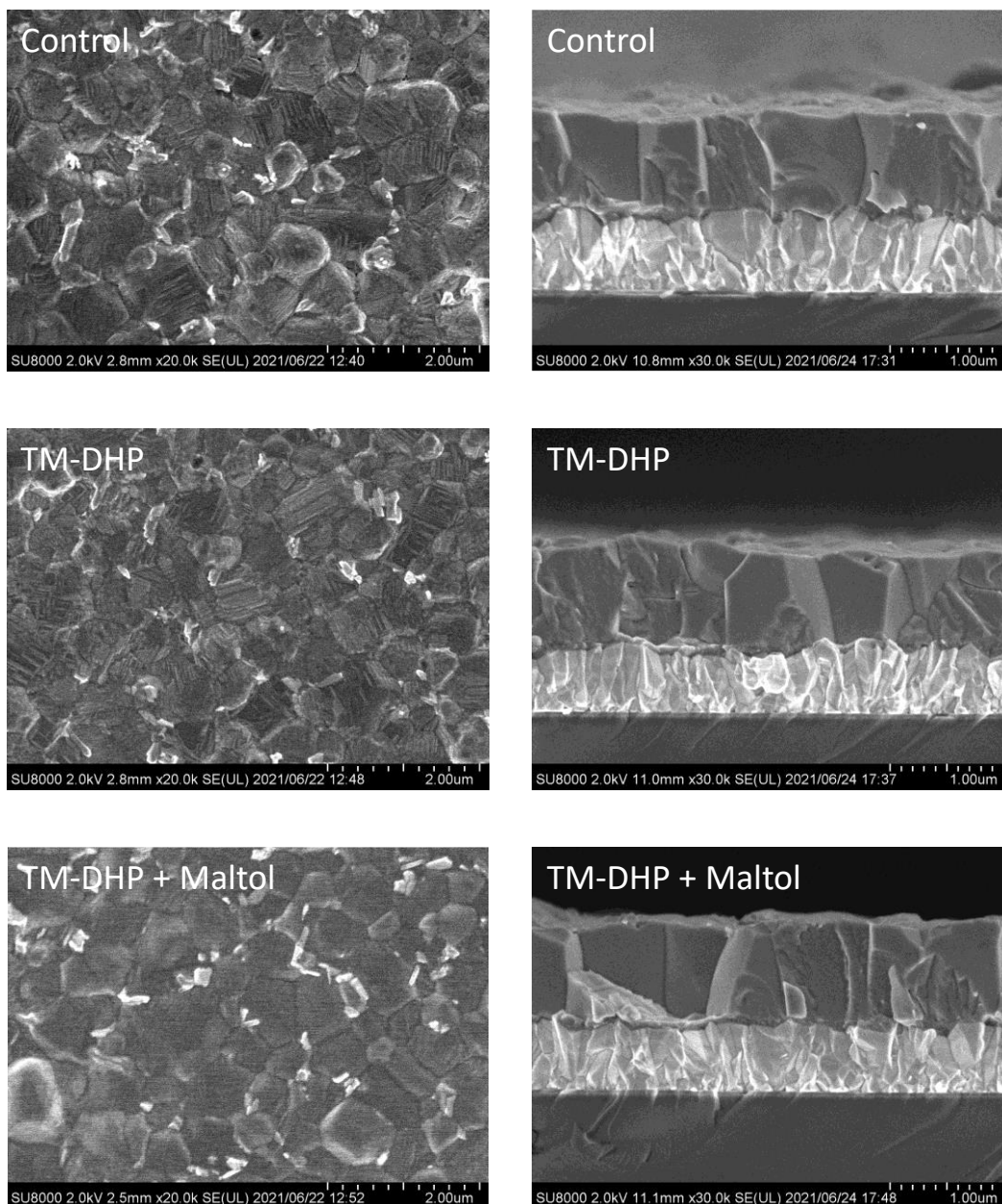


Figure S10. Top-view (left) and cross-sectional (right) SEM images of the perovskite films fabricated on PEDOT:PSS-coated FTO substrates.

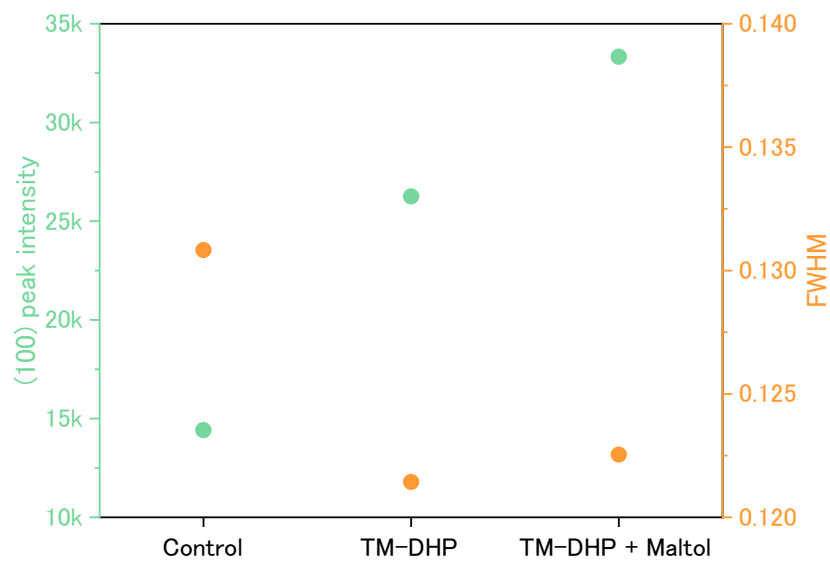


Figure S11. XRD peak intensity and FWHM of (100) peak for the perovskite films.

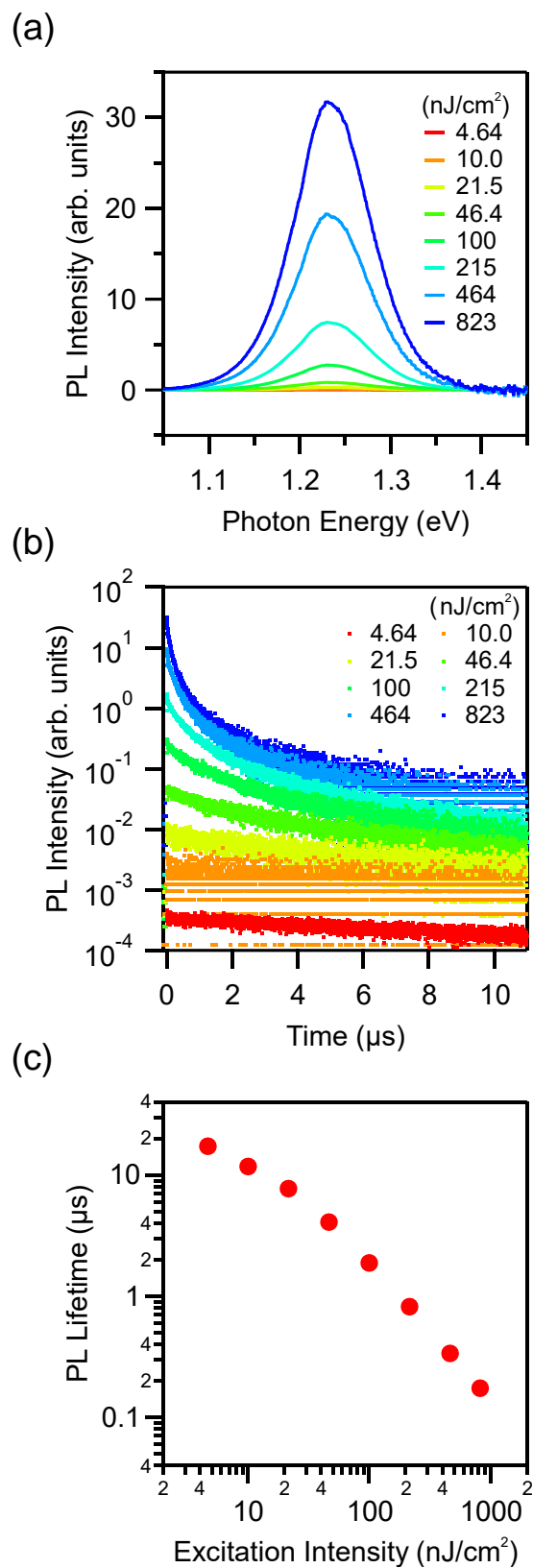


Figure S12. (a) PL spectra and (b) TRPL decay curves for the perovskite film with TM-DHP treatment under different excitation intensities. (c) PL lifetime as a function of excitation intensity.

The charge carrier lifetimes are strongly dependent on the excitation intensity,³ becoming longer at lower excitation intensities (Figure S12). When the excitation intensity was reduced to 2.8×10^{10} photons cm^{-2} , the lifetime increased to 28 μs (Figure S13).

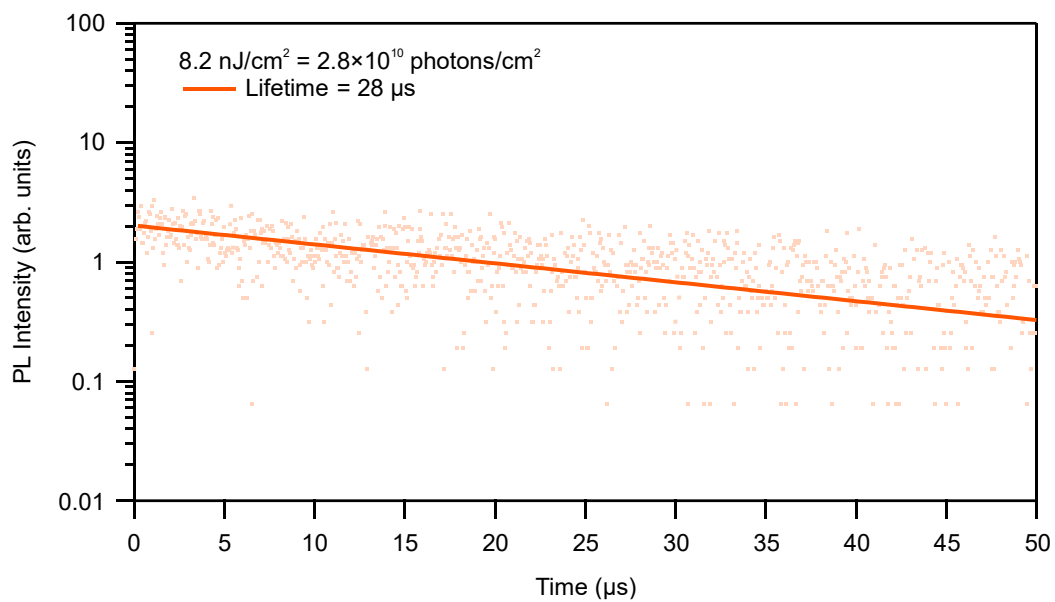


Figure S13. TRPL decay of the perovskite film treated with TM-DHP and maltol.

The measured charge carrier lifetimes depend on the charge carrier density, which in turn depends on the excitation intensity. Figure S12 shows the PL lifetime dependence with the excitation intensity. The PL lifetime of 7.4 μs was obtained at the excitation intensity of 3.5×10^{11} photons cm^{-2} , while the TRMC lifetime at a similar excitation intensity (6.4×10^{11} photons cm^{-2}) was 8.5 μs (Figure S15). When the intensity of the PL excitation is reduced to 2.8×10^{10} photons cm^{-2} , the measured lifetime increases to 28 μs (Figure S13), while that of TRMC under a photon flux of 6.4×10^{10} photons cm^{-2} for $t = 19.5$ μs (Figure S14a). The charge carrier lifetimes observed in the TRMC experiments also depends on whether holes or electrons are being observed since the HTM and ETM layers influence the charge carrier density in the perovskite film. For holes, which are assumed to be the majority carrier, the effect of the C_{60} layer is to reduce electron density in the perovskite layer. The observed lifetime increases substantially as there are almost no free electrons left for the hole to recombine with (161 μs , Figure S14b). When electron lifetimes are monitored by addition of a PEDOT:PSS layer to reduce hole density in perovskite layer, the lifetime is reduced as electrons are the minority carrier (2.7 μs , Figure S14c).

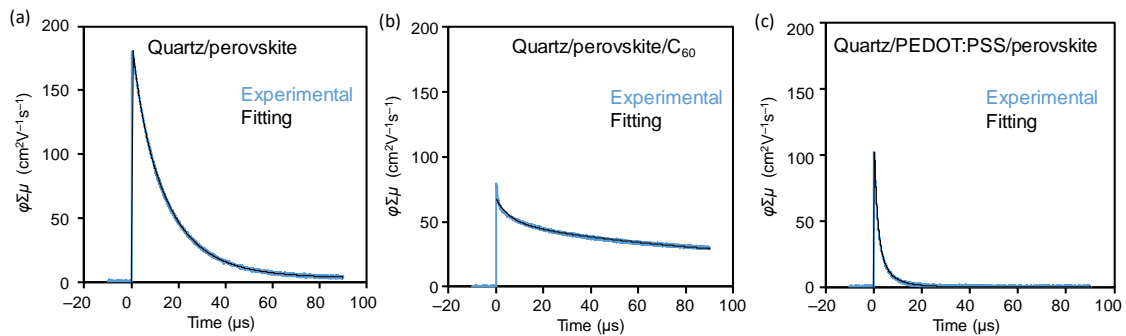


Figure S14. TRMC transients of Pb-Sn perovskite with TM-DHP and maltol treatment ($\lambda_{\text{ex}} = 500$ nm, incident photon density $I_0 = 6.4 \times 10^{10}$ photons cm^{-2}). (a) Perovskite on a quartz substrate, (b) quartz/perovskite/ C_{60} , and quartz/PEDOT:PSS/perovskite. The blue and black lines are the experimental and analytical curves, respectively. The latter is the double exponential function: $A_1 \exp(-k_1 t) + A_2 \exp(-k_2 t)$, where the effective lifetime (τ_{eff}) is calculated through $\tau_{\text{eff}} = (A_1 k_1^{-1} + A_2 k_2^{-1}) / (A_1 + A_2)$. The maxima of $\phi \Sigma \mu$ transients in (a), (b), and (c) are ~ 180 (sum of hole and electron), 70 (hole), and 110 $\text{cm}^2 \text{V}^{-1} \text{s}^{-1}$ (electron), respectively. The τ_{eff} values of (a), (b), and (c) are 19.5, 161, and 2.7 μs , respectively.

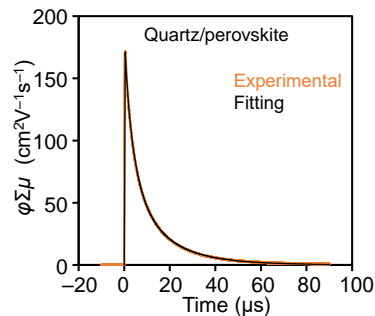


Figure S15. TRMC transient of $\text{Cs}_{0.1}\text{FA}_{0.6}\text{MA}_{0.3}\text{Sn}_{0.5}\text{Pb}_{0.5}\text{I}_3$ perovskite film with TM-DHP and maltol treatment ($\lambda_{\text{ex}} = 500$ nm, incident photon density $I_0 = 6.4 \times 10^{11}$ photons cm^{-2}). The τ_{eff} values is 8.5 μs .

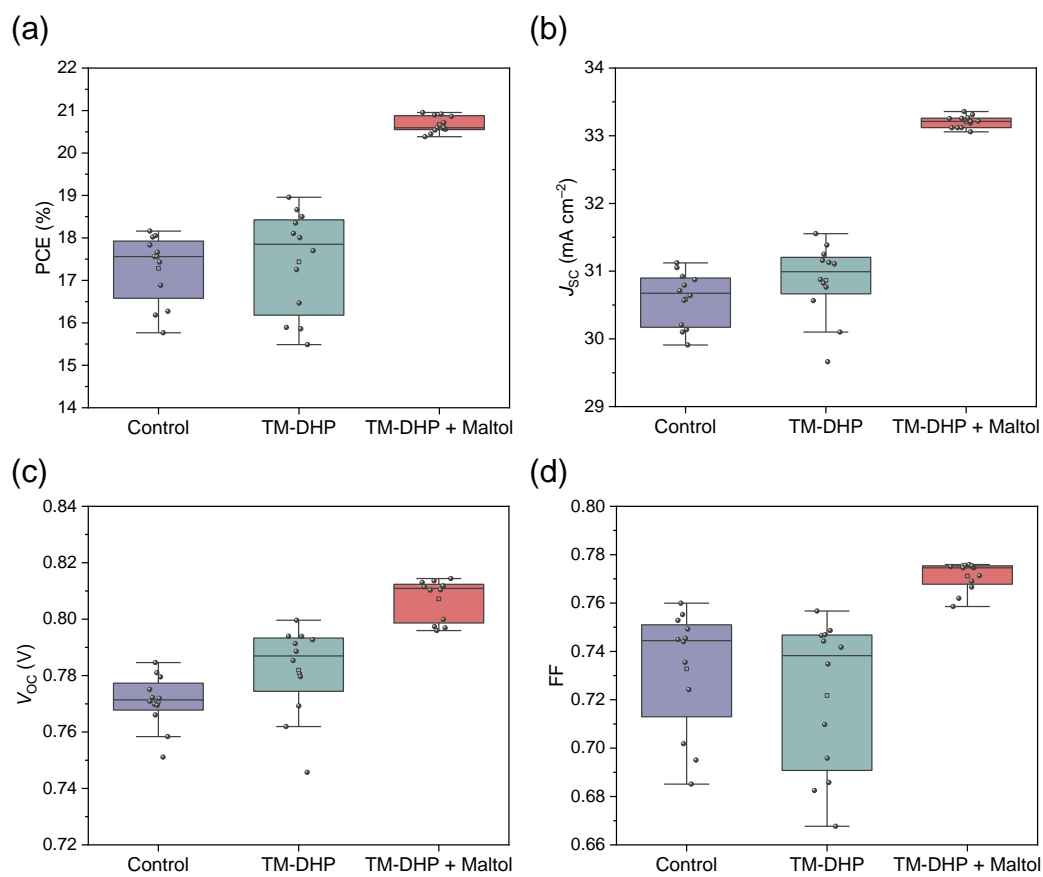


Figure S16. Performance parameters of the PSCs obtained from the same batch with six cells for each condition.

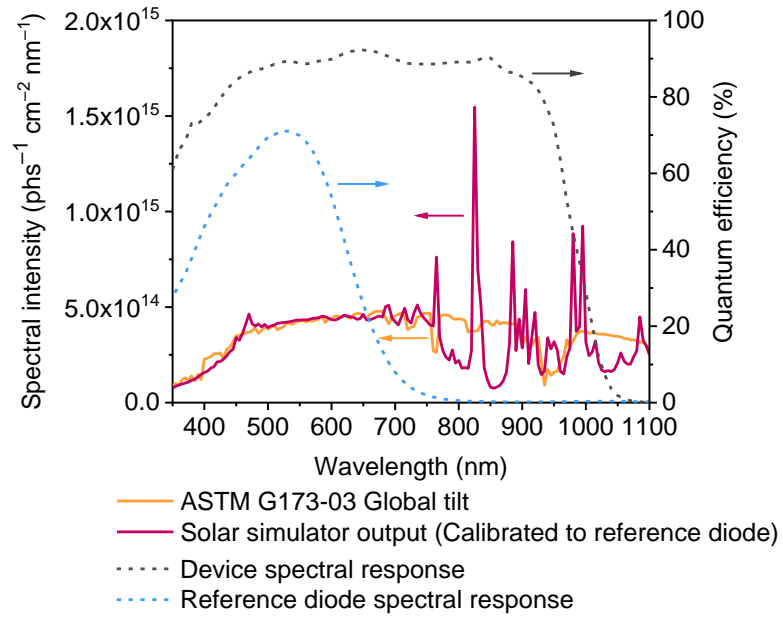


Figure S17. Data used to calculate the spectral mismatch, $m = 1.027$: The measured IPCE of the Pb–Sn test device and calibration diode, as well as the spectral intensity of the solar simulator (BUNKOUKEIKI OTENTO SUN) and AM1.5G reference.

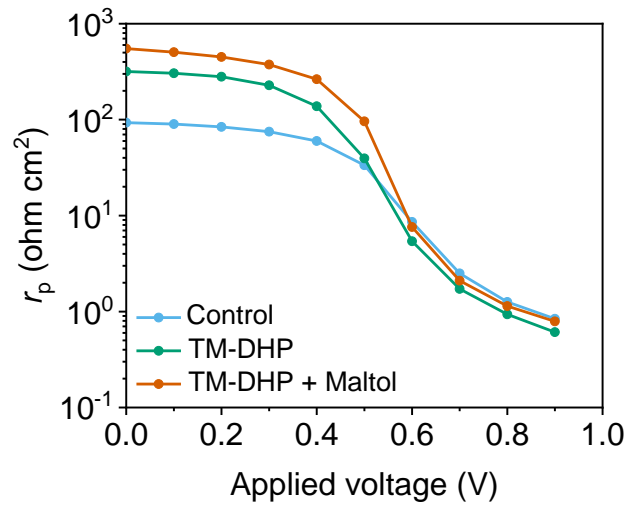


Figure S18. The parallel resistance, r_p , as a function of applied bias voltage, obtained from the fitting analysis of the complex impedance data. At low voltages the parallel resistance is determined by the shunt resistance of the perovskite layer, and follows a clear ascending order for Control, TM-DHP, and TM-DHP + Maltol devices, respectively. The trend is maintained until about 0.5 V, after which the parallel resistance is dominated by the recombination resistance of the diode element. No clear trends are observed for the three curves within this region.

Table S2. The hole and electron trap densities estimated from the SCLC measurements.

Sample ^a	Hole-only devices ^b		Electron-only devices ^c	
	V_{TFL}/V	N_{trap} (hole)/cm ⁻³	V_{TFL}/V	N_{trap} (electron)/cm ⁻³
Control	0.62	2.9×10^{15}	0.10	4.5×10^{14}
TM-DHP	0.54	2.4×10^{15}	0.10	4.5×10^{14}
TM-DHP + Maltol	0.14	6.3×10^{14}	0.08	3.6×10^{14}

^aThe thickness of the perovskite layer in the devices is 890 ± 68 nm.

^bThe architecture of hole-only device is FTO/PEDOT:PSS (50 nm)/perovskite/PTAA (80 nm)/Ag (100 nm).

^cThe architecture of electron-only device is FTO/C₆₀ (30 nm)/perovskite/C₆₀ (30 nm)/Ag (100 nm).

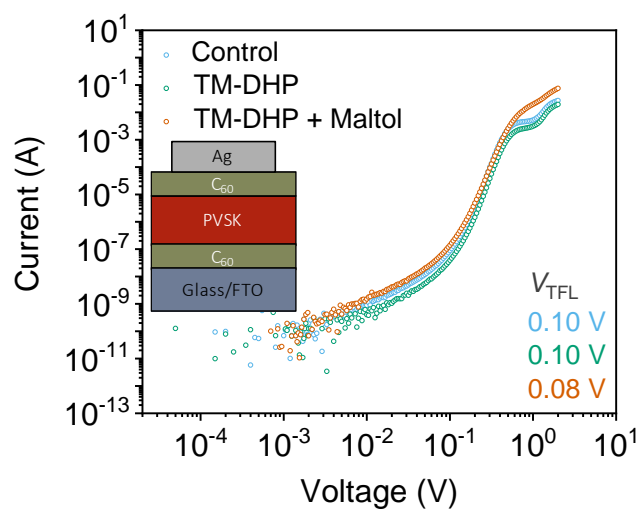


Figure S19. Dark current–voltage curves of the electron-only devices with the architecture of FTO/C₆₀/perovskite/C₆₀/Ag.

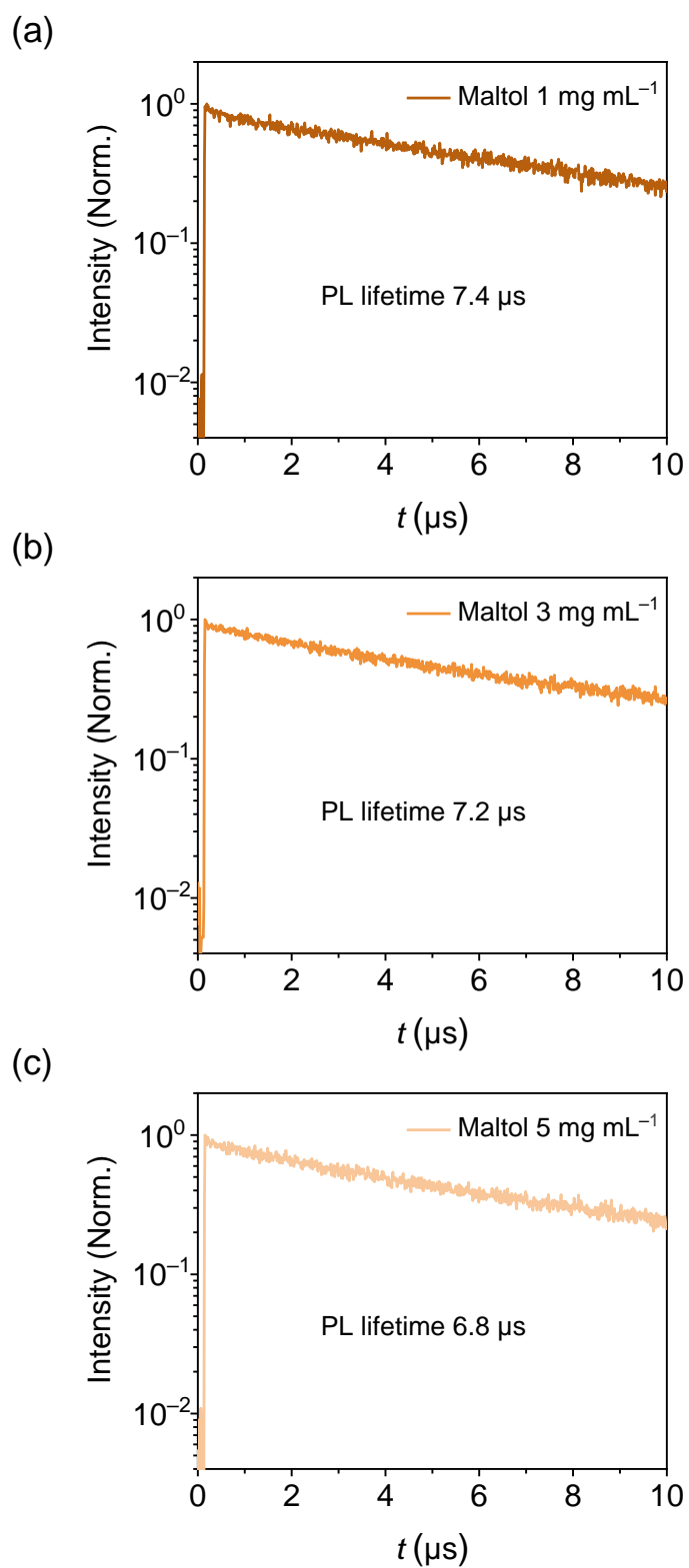


Figure S20. TRPL decay curves of the perovskite films treated with TM-DHP and different amount of maltol.

Not all the molecules that have strong affinities for Sn can be applied for the passivation of the Sn-containing perovskite films, however. We also need to consider about the other properties of the molecules, such as the basicity or polarity. As shown in the SEM image (Figure S19a), the surface of the perovskite, however, seems disastrously dissolved by the kojic acid after the post treatment. The performance of the PSCs decreased accordingly (Figure S19b).

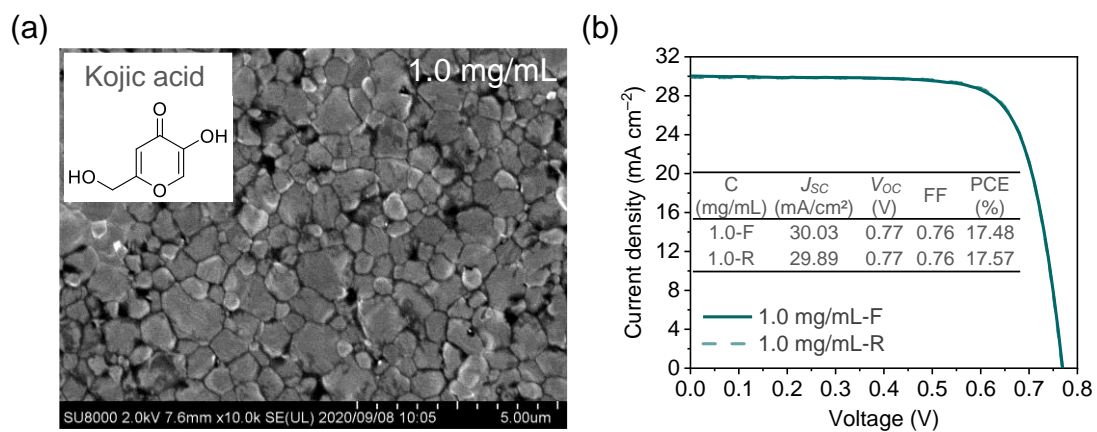


Figure S21. (a) Top-view SEM image of the perovskite films post-treated with 1 mg mL⁻¹ kojic acid in toluene, insertion shows the chemical structure of kojic acid. (b) J - V curves of the PSCs fabricated with kojic acid.

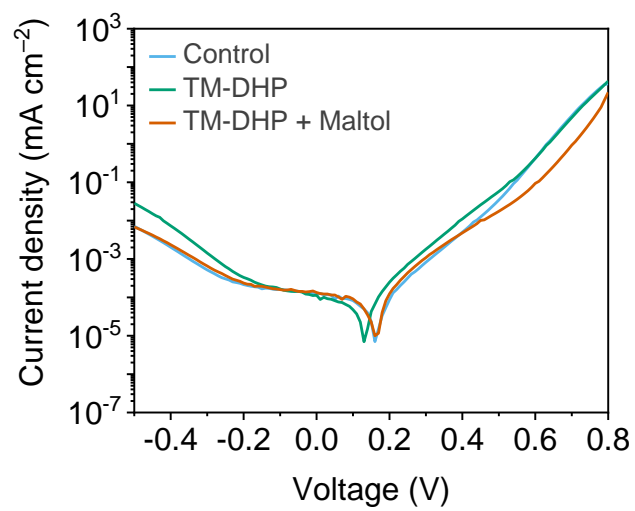


Figure S22. Dark J - V curves of the devices.

Under maximum power point tracking (MPPT) operation at AM1.5G in inert atmosphere, the output efficiency of the unencapsulated maltol-treated device fell to 50% of its initial value after 10 h (Figure S21). Despite the passivation by the maltol, and the high initial quality of the perovskite layer, device stability remains limited, and is an issue that we must examine carefully in future work.

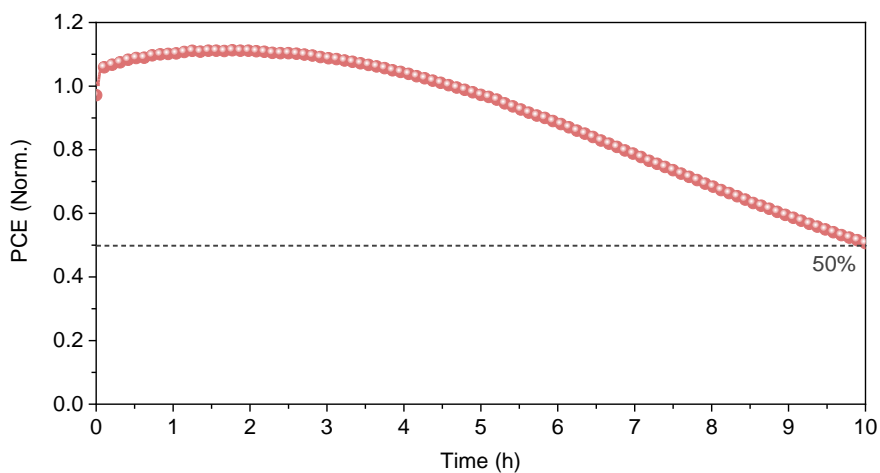


Figure S23. Maximum power point tracking (MPPT) of the representative device prepared with TM-DHP and maltol treatment under AM 1.5G illumination without ultraviolet cut filter in N₂-filled glovebox.

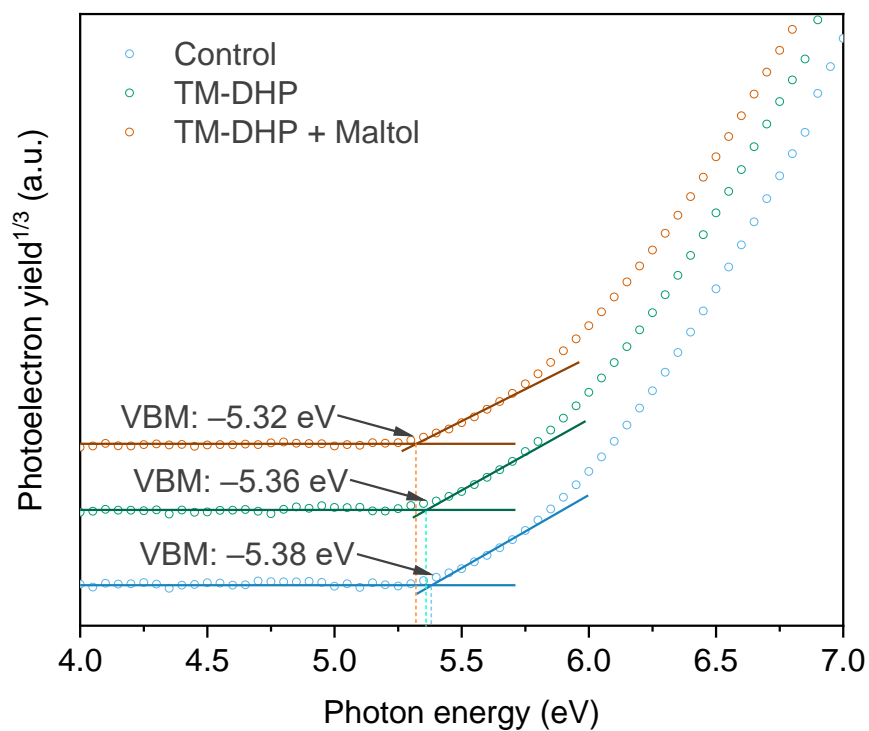


Figure S24. Photoelectron yield spectroscopy (PYS) results showing the valence band maxima (VBM) for the perovskite films.

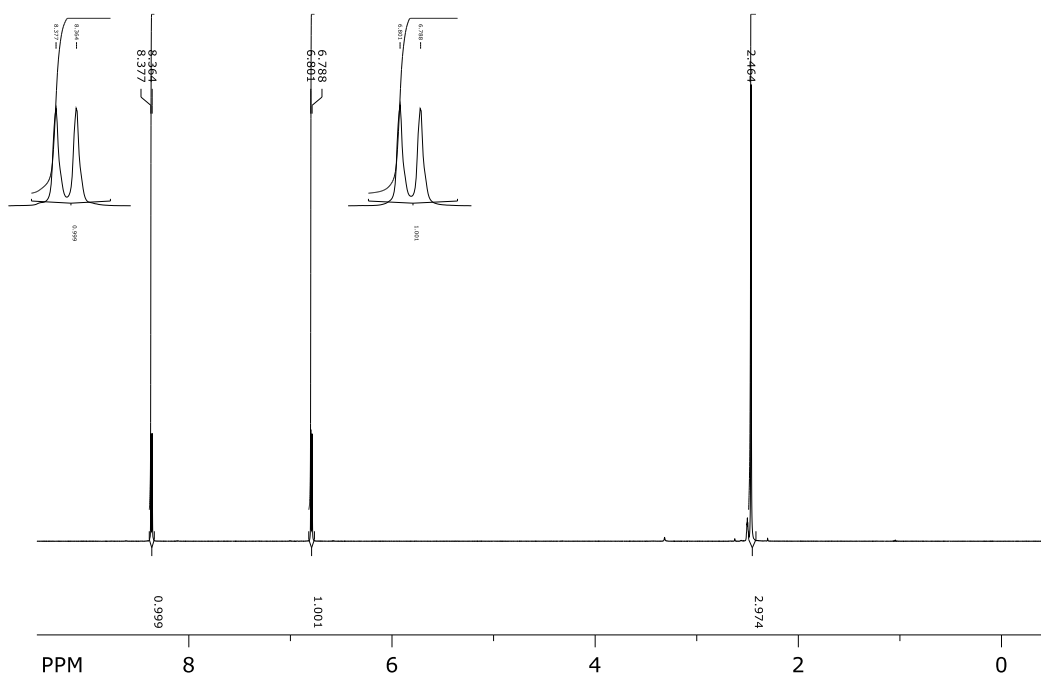


Figure S25. ^1H NMR (400 MHz, $\text{DMSO-}d_6$) of SnI(maltol) .

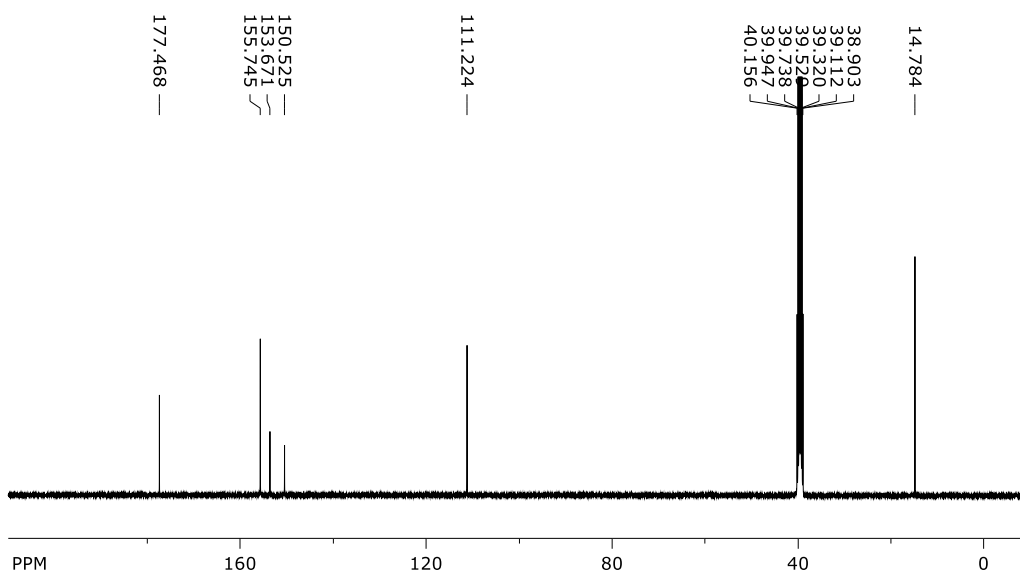


Figure S26. ^{13}C NMR (101 MHz, $\text{DMSO-}d_6$) of SnI(maltol) .

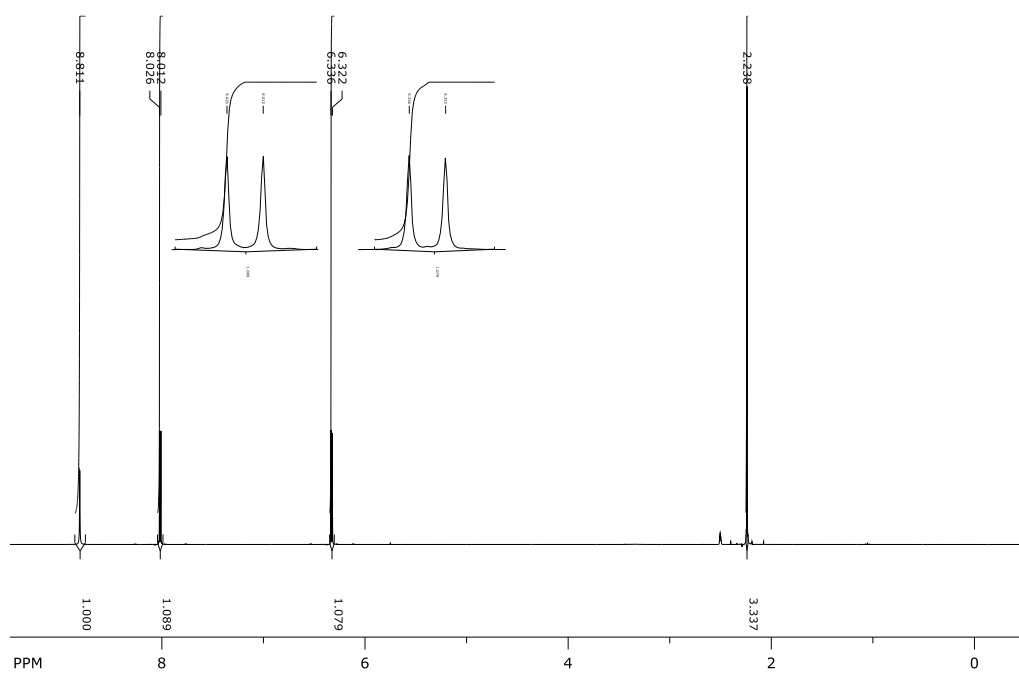


Figure S27. ^1H NMR (400 MHz, $\text{DMSO}-d_6$) of maltol.

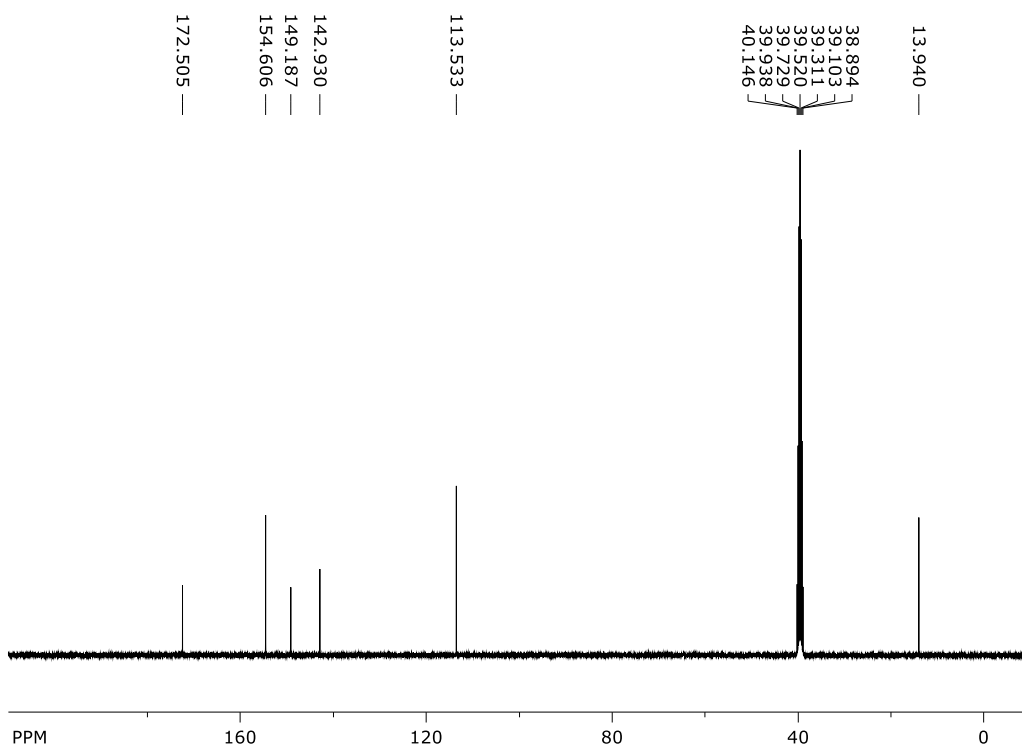


Figure S28. ^{13}C NMR (101 MHz, $\text{DMSO}-d_6$) of maltol.

References

1. T. Nakamura, S. Yakumaru, M. A. Truong, K. Kim, J. Liu, S. Hu, K. Otsuka, R. Hashimoto, R. Murdey, T. Sasamori, H. D. Kim, H. Ohkita, T. Handa, Y. Kanemitsu and A. Wakamiya, *Nat. Commun.*, 2020, **11**, 3008.
2. G. Sheldrick, *Acta Crystallogr. A*, 2015, **71**, 3-8.
3. Y. Yamada, T. Nakamura, M. Endo, A. Wakamiya and Y. Kanemitsu, *J. Am. Chem. Soc.*, 2014, **136**, 11610-11613.